UILU-ENG-83-3604

FCP Report No. 48

ESTIMATING THE FATIGUE RESISTANCE OF TENSILE-SHEAR SPOT WELDS

by

F. V. Lawrence, Jr.

P. C. Wang

N.-J. Ho

H. T. Corten

A Report of the

FRACTURE CONTROL PROGRAM

College of Engineering, University of Illinois

Urbana, Illinois 61801

March 1983

TABLE OF CONTENTS

ABSTRACT

An empirical method which is based principally on estimates of the fatigue crack initiation life (N_I) has been developed which predicts the fatigue resistance of tensile-shear spot welds in the long life regime. The method uses Basquin's law and Peterson's equation to estimate N_I and thus is founded on the fatigue behavior of smooth specimens and modelling of the fatigue notch size effect. The fatigue notch factor (K_f) required in this analysis was obtained from Pook's relationships for the stress intensity factors of tensile-shear spot welds. Preliminary results from a three-dimensional finite element elastic stress analysis agree well with the estimates of elastic stress concentration factor obtained using Pook's relationships. Estimates of N_I are added to estimates of the fatigue crack propagation life N_p to obtain the total fatigue life (N_T) but in the long life regime N_p can usually be neglected. The improvement of tensile-shear spot weld fatigue resistance through manipulation of geometry and material property variables are discussed with the aid of the model. The model predicts that nugget diameter, sheet thickness, and residual stress control offer the best possibilities for fatigue life improvement.

1. THE FATIGUE RESISTANCE OF TENSILE-SHEAR SPOT WELDS

The fatigue resistance of tensile-shear spot welds depends upon: the geometry of the weldment, that is, its nugget diameter (D), sheet widths (W) and thickness (t); upon material properties of the sheet and the weld heat-affected-zone; and upon the load history. The influence of these many variables has been summarized by Davidson (1). Studies performed by the authors at the University of Illinois confirm the results reported (1,2) that material properties seem to influence the fatigue resistance of tensile-shear spot welds to a very small degree. Galvanization of the sheets prior to spot welding also does not seem to alter the fatigue resistance. Welding conditions were found to diminish significantly the fatigue resistance in the case of underwelding but overwelding (expulsion) did not greatly alter the fatigue resistance.

Figure 1 shows typical results from the fatigue testing program which has been carried out at the University of Illinois. This program has studied the influence of welding conditions on tensile-shear, coach-peel, and cross-tension welds of SAE 1006 and SAE 960x in both the bare and galvanized state. All tests were performed under ambient laboratory conditions using a constant amplitude load controlled ($R = 0$) load history at a frequency of 7 to 10 Hz. The important results of this study for the tensile-shear welds are summarized in the load-life diagrams of Figs. 2 and 3 which contain best fit lines to the test data. Figure 2 shows the influence of weld cycle. The welding parameters are summarized in Table 1. Figure 3 shows that neither material properties nor galvanization seem to greatly influence the fatigue resistance of tensile-shear spot welds. The mechanical properties of the materials considered in this study are listed in Table 2.

In the following sections, the development of an empirical method for

estimating the fatigue resistance of tensile-shear spot welds will be described. The predictions made using this model are compared with the experimental results of this study and those reported by Davidson and Imhof (2). Finally, the developed model is used to explore the most effective ways to improve tensile-shear spot weld fatigue resistance.

2. THE INITIATION-PROPAGATION MODEL FOR PREDICTING THE FATIGUE RESISTANCE OF WELDS

The initiation-propagation (I-P) model (3) is a hybrid, semi-empirical model for estimating weldment fatigue resistance which predicts the total fatigue life (N_T) by combining estimates of the fatigue crack initiation life (N_I) and the fatigue crack propagation life (N_p).

$$N_T = N_I + N_p \tag{1}$$

The initiation-propagation (I-P) model has the disadvantage of requiring two separate analyses but circumvents the small crack problem through the use of smooth specimen fatigue data to estimate the life devoted to fatigue crack initiation and small crack growth, a period termed the fatigue crack initiation life (N_I).

For long life fatigue ($N_I > 10^6$ cycles), cyclic hardening and softening effects can usually be ignored, and generally elastic conditions may be assumed. In such cases, N_I may account for the major portion of the total fatigue life and can be estimated using the empirical Basquin relationship (3):

$$\sigma_a = (\sigma'_f - \sigma_o)\ [2N_I]^b \tag{2}$$

where σ_a is the stress amplitude, σ_f' is the fatigue strength coefficient, σ_o is the mean stress including weld residual and remote mean stresses (after the initial set-up cycle), $2N_I$ is the reversals to fatigue crack initiation, and b is the fatigue strength exponent. The notch-root stress amplitude, the stress at the critical region in the weld (weld toe or internal defect), can be taken as $K_f \Delta S/2$ so that Eq. 2 becomes:

$$\frac{\Delta S}{2} K_f = (\sigma_f' - \sigma_o) [2N_I]^b \tag{3}$$

where ΔS is the remote stress range, and K_f is the fatigue notch factor (also K_{fmax}).

A difficulty in proceeding with the calculation suggested by Eq. 3 is determining the appropriate value of K_f for the weld toe. This difficulty arises from the fact that the notch-root radius of a discontinuity such as a weld toe is unknown and variable. Microscopic examination of weld toes reveals that practically any value of radius can be observed; thus, notches such as weld toes must be considered to have all possible values of notch-root radius which conclusion has led to the idea of a maximum value of K_f for a given weld shape, K_{fmax} (3). K_f can be estimated using Peterson's equation:

$$K_f = 1 + \frac{K_t - 1}{1 + \frac{a}{r}} \tag{4}$$

where K_t is the elastic stress concentration factor, $\underline{a}$ is a material parameter ($\approx 1.08 \times 10^5 S_u^{-2}$), for steels (mm), r is the notch root radius (mm), and S_u is the ultimate strength (MPa).

The elastic stress concentration factor (K_t) can be estimated using finite element methods as a function of assumed notch root radii (r) or a

given weld of a given weld geometry. Assuming a general form for K_t

$$K_t = 1 + \alpha(t/r)^{1/2} \tag{5}$$

where α is a constant determined by the weld geometry and type of loading and t is the plate thickness. Substituting this expression into Eq. 4 and differentiating with respect to (r) leads to the maximum value of K_f, K_{fmax}:

$$K_{fmax} = 1 + (\alpha/2)(t/\underline{a})^{1/2} \tag{6}$$

for steel. Because $\underline{a}$ is dependent upon the ultimate strength (S_u), higher strength steels will have higher values of K_{fmax} for the same weld shape. The value of K_{fmax} also depends upon the shape of the weld and the type of loading to which it is subjected (α) and upon the size or scale of the weldment (t).

An expression for the fatigue strength of a weld under a given loading condition (R) and at long lives can be obtained by combining Eq. 3 and the concept of K_{fmax} (Eq. 6):

$$\frac{\Delta S}{2} = \frac{(S_u + 345 - \sigma_r)(2N_I)^b}{K_{fmax}\left[1 + \frac{1 + R}{1 - R}(2N_I)^b\right]} \tag{7}$$

where $\Delta S/2$ is the fatigue strength at a life of N_I, K_{fmax} is given by Eq. 6, S_u is the ultimate tensile strength ($\sigma_f' \approx S_u + 345$), ($\sigma_r$ is the residual stresses (taken as $+ S_y$, 0, $- S_y$) and b is the fatigue strenth exponent ($\approx -\frac{1}{6}\log 2(1 + 345/S_u)$), R is the stress ratio of the load history (S_{min}/S_{max}).

3. ESTIMATION OF ELASTIC STRESS CONCENTRATION FACTORS (K_T) FOR SPOT WELDS

Expressions for the stress intensity factors sharp cracks have been modified to predict the elastic stress concentration factor (K_t) associated with cracks having a finite radius (4). These corrections are applicable to all crack-tip stress fields and thus can be applied to the expressions of Pook (5) for the stress intensity factors of tensile-shear spot welds:

$$K_I = \frac{P}{D^{1.5}} \{.964\ (D/t)^{.397}\}$$

$$K_{II} = \frac{P}{D^{1.5}} \{.798 + .458\ (D/t)^{.710}\} \qquad (D/t < 10) \qquad (8)$$

where P is the load applied to spot weld, D is the nugget diameter, t is the sheet thickness. The above stress intensity factor expressions for point A in Fig. 4 are based on small deformation elasticity; and, thus, finite deformations such as nugget rotation are neglected. A more complex set of expressions for stress intensity factors which include the effects of nugget rotation have also been given by Pook (6). The effects of nugget rotation have been found to be small for the purposes of this study of long life fatigue.

The hyperbolic blunt crack shown has a finite crack-tip (r). A polar system of coordinates centered at 0 is used and $\rho \cos \theta = (\eta+1/2)r$. $\rho \sin \theta = \lambda r$. Where η and λ are non-dimensional parameters which define the position of a point relative to the crack tip: see Fig. 5

The stress field ahead of the blunt crack tip is (4):

For Mode I :

$$\begin{matrix}\sigma_x \\ \sigma_y \\ \tau_{xy}\end{matrix} = \frac{K_I}{(2\pi\rho)^{1/2}} \left[\begin{matrix} f_1(\theta) \\ f_2(\theta) \\ f_3(\theta)\end{matrix} - \frac{r}{2\rho} \begin{matrix}\cos\frac{3}{2}\theta \\ \cos\frac{3}{2}\theta \\ \sin\frac{3}{2}\theta\end{matrix}\right]$$

For Mode II :

$$\begin{matrix}\sigma_x \\ \sigma_y \\ \tau_{xy}\end{matrix} = \frac{K_{II}}{(2\pi\rho)^{1/2}} \left[\begin{matrix} f_4(\theta) \\ f_5(\theta) \\ f_6(\theta)\end{matrix} + \frac{r}{2\rho} \begin{matrix}\sin\frac{3}{2}\theta \\ \sin\frac{3}{2}\theta \\ \cos\frac{3}{2}\theta\end{matrix}\right] \qquad (9)$$

where :

$$f_1(\theta) = \cos\frac{\theta}{2}\left[1 - \sin\frac{\theta}{2}\sin\frac{3}{2}\theta\right]$$

$$f_2(\theta) = \cos\frac{\theta}{2}\left[1 + \sin\frac{\theta}{2}\sin\frac{3}{2}\theta\right]$$

$$f_3(\theta) = \sin\frac{\theta}{2}\cos\frac{\theta}{2}\cos\frac{3}{2}\theta$$

$$f_4(\theta) = -\sin\frac{\theta}{2}\left[2 + \cos\frac{\theta}{2}\cos\frac{3}{2}\theta\right]$$

$$f_5(\theta) = \sin\frac{\theta}{2}\cos\frac{\theta}{2}\cos\frac{3}{2}\theta$$

$$f_6(\theta) = \cos\frac{\theta}{2}\left[1 - \sin\frac{\theta}{2}\sin\frac{3}{2}\theta\right]$$

The maximum tangential stress along the interior surface of the blunt crack tip due to a remotely applied load P is :

$$\sigma_t = \frac{K_I}{(\pi r)^{1/2}}\cos^2\frac{\theta}{2} - \frac{K_{II}}{(\pi r)^{1/2}}\sin\theta \qquad (10)$$

when one substitutes the stress intensity factors of Pook (Eq. 3) into Eq. 10 and locates the maximum value of σ_t, it is found to occur at an angle θ of -48° for sheet thicknesses in the range of 1 to 2 mm. The initial angle of crack growth from this point of maximum stress is predicted to be 66° from the horizontal: see Fig. 5.

If one defines the elastic stress concentration factor (K_t) as the ratio of the peak notch tip stress (σ_t at θ = -48°) to the remote stress (P/wt), then K_t for a tensile-shear spot weld becomes from Eqs. 8 and 10:

$$K_t = \frac{Wt}{(\pi r)^{1/2} D^{1.5}} \{1.61\ (D/t)^{.397} + .593 + .340\ (D/t)^{.710}\} \quad (11)$$

4. PRIMITIVE FINITE ELEMENT STRESS ANALYSIS OF TENSILE SHEAR SPOT WELD

4.1 Mesh and Mesh Drawing

The geometry of the simulated spot weld specimen was modeled by subdividing it into a mesh of 20-node, isoparametric, three-dimensional elements. Accurate determination of the stress distribution in areas close to the notch root of the weld was performed using a finer mesh in areas close to these regions. Figures 6, 7 and 8 show the finite element representation for this particular geometry of spot weld. Due to the symmetry of the specimen (of single tensile-shear spot weld), Fig. 6 shows the coarse mesh drawing for only one-half of the specimen. The nugget area is enlarged and is shown in Fig. 7. Further enlargement of the mesh near the notch root can be seen in Fig. 8.

In three-dimensional finite element analysis for a complex geometry such as a spot weld, it is impossible to draw a 3-D mesh by hand without any error in numbering the nodes or giving them correct coordinates. A computer pro-

gram which can help to do the numbering and coordinate checking has been developed to generate and plot 3-D finite element mesh from a 2-D mesh. This program saves tremendous manpower and valuable time. A further advantage of the computer program is its accuracy which could never be achieved by hand.

4.2 FEM Results

The primitive results of 3-D FEM stress analysis for a single tensile-shear spot weld with a large nugget size (D/t = 10, W/D = 3) can be seen in Figs. 9, 10 and 11. The principal stress flow around the nugget circumference in the Z plane (containing X and Y axes) is shown in Fig. 9. Maximum principal stress occurs at point A (see Fig. 9). and extends to 20 degrees beyond point A; then, it decreases rapidly near point C (also see Fig. 9). In the case of pull-out failure, the crack starts at the point A, then it propagates along the nugget circumference to some extent and propagates into base metal until final pull-out failure. The projection of the crack propagation path onto the Z plane (top view of the spot weld) seems to follow the principal stress flow direction. Figure 10 shows the principal stress flow at the notch root in Y plane (containing X and Z axes and point A). The maximum principal stress occurs at a point with its direction away from the Z axis by 20 degrees and decreases rapidly near the tip of the notch root.

The principal stress flow pattern also demonstrates the pull-out failure. The fatigue crack starts at the point with maximum principal stress instead of at the notch tip and propagates outward through the main plate. The value of the maximum principal stress and the place where it occurs for this particular geometry are close to the calculations made using Pook's stress intensity factor and blunt tip stress field model (Eq. 11). The maximum local stress from FEM results for the geometry (t/r = 8, D/t = 10 and W/D = 3) is

about 1000 units for 100 units of applied stress. The elastic stress concentration (K_t) for a single tensile-shear spot weld is given by Eq. 11. The result using Eq. 11 is 953 units for 100 units of applied stress. Thus, the FEM results agree well with the predictions of Eq. 11. However, the FEM can provide additional information on the variation of the stress outward from the point of maximum principal stress along the crack path. Fig. 11 shows the variation of the stress outward from the notch surface (necessary for determination of Np).

5. APPLICATION OF THE I-P MODEL TO SPOT WELDS

To apply the I-P model to spot welds, it was necessary to develop an expression for the fatigue notch factor (K_f or K_{fmax}) similar to Eq. 6. To do this, the expressions for spot weld stress concentration factor (Eq. 11) was used. Since K_{fmax} is K_f evaluated for a notch root radius (r) equal to the material constant ($\underline{a}$) in Peterson's equation (Eq. 4), K_{fmax} for tensile-shear spot welds is ($K_t \approx K_t - 1$):

$$K_{fmax} \cong 1 + 2.41 \times 10^{-3} W S_u D^{-1} t^{1/2} f(\tfrac{t}{D}) \text{ (MPa-mm units)} \qquad (12)$$

$$f(\tfrac{t}{D}) = .569\,(\tfrac{t}{D})^{.103} + .209(\tfrac{t}{D})^{.5} + .12(\tfrac{t}{D})^{-.21}$$

t/D	.1	.2	.3	.4	.5
f(t/D)	.710	.744	.772	.795	.816

Since f(t/D) is nearly constant in the ranges of t/D of practical interest (t/D = .2 to .3):

$$K_{fmax} \cong 1 + 1.81 \times 10^{-3} S_u D^{-1} t^{1/2} \quad \text{(MPa-mm units)} \tag{13}$$

Observed and predicted values of load range at 2×10^6 cycles are compared in Table 2 and Fig. 12. Microhardness measurements in the spot weld HAZ were used to determine S_u HAZ required in the predictions. Since SAE 990x and SAE 960x have similar mechanical properties, the S_u HAZ values determined for the SAE 960x of this study were used to predict the load ranges for the results reported by Davidson and Imhof (2). Except for one test result, the experimental results and predictions made using Eqs. 7 and 13 agree within 25%: see Fig. 12. Predictions of total fatigue life (N_T) were made by adding separate estimates of N_I (Eq. 7) and the fatigue crack propagation life (N_p). As seen in Figs.13 and 14, the agreement between the predictions and experiment are reasonably good for lives greater than 10^6 cycles; however at lives less than 10^6 cycles where fatigue crack propagation is expected to dominate, the modeling of fatigue crack growth by the two-dimensional stress analysis which was used here (7) underestimates N_p.

6. IMPROVEMENT OF SPOT WELD FATIGUE RESISTANCE

6.1 Factors Influencing Fatigue Strength

The I-P model relationships developed for spot welds can be used to explore ways to improve their fatigue performance. Equation 7 predicts the remote stress range which would result in a fatigue life of $2N_I$.

$$\frac{\Delta S}{2} = \frac{(S_u + 345 - \sigma_r)\ (2N_I)^b}{K_{fmax}\left[1 + \frac{1 + R}{1 - R}\ (2N_I)^b\right]} \tag{7}$$

where S_u is the ultimate tensile strength of the heat-affected zone region in which crack initiation and early growth occurs. The range of load which results in the life N_I for a tensile-shear spot weld can be estimated recalling that

$$\Delta P = Wt\ \Delta S \tag{14}$$

so from Eqs. 7 and 13 (MPa-mm units):

$$\Delta P = \left[\frac{2\ Wt\ (S_u + 345 - \sigma_r)}{1 + \frac{2.41 \times 10^{-3}\ WS_u t^{1/2}}{D}\ f\left(\frac{t}{D}\right)}\right] \times \left[\frac{(2N_I)^b}{1 + \frac{1 + R}{1 - R}\ (2N_I)^b}\right] \tag{15}$$

$$\Delta P = f(W,\ t,\ D,\ S_u,\ \sigma_r,\ R,\ N_I) \tag{16}$$

where $b \approx -1/6 \log 2(1 + 345/S_u)$.

Thus, the range in load (ΔP) for a given life ($N_I > 10^6$) depends principally upon geometric variables (W, t, D), upon material properties (S_u(HAZ), S_y(BM) $\approx \sigma_r$), and upon the imposed mean stress, that is, the stress ratio (R).

6.2 The Predicted Effects of Geometry

The predicted effects of sheet width (W), thickness (t), and nugget diameter (D) on ΔP at 10^7 cycles are shown in Figs.15-17 for SAE 1006 and HSLA spot welds. Sheet width (W) has only a modest influence. Sheet thickness (t) causes an increase in ΔP but increasing sheet thickness in order to improve

the fatigue strength of spot welds is probably not a practical suggestion. The load range (ΔP) is proportional to $t^{1/2}$. Nugget diameter (D) causes the largest changes in ΔP and would seem to be the most direct and practical means of increasing fatigue strength through changes in geometry. The load range is proportional to D.

Another feature of spot weld geometry which could cause changes in fatigue resistance is alteration of the notch root geometry through expulsion, too high clamping forces during welding or poor fit-up. It is possible that such non-K_{fmax} conditions might occur, and the consequences of these possibilities should be studied.

6.3 The Predicted Effects of Material Properties

The fatigue strength or load ranges (ΔP) for a given life will depend on the S_u of the spot weld HAZ in a complex way as predicted by Eq. 15. The notch root residual stresses (σ_r) should also be controlled by material properties if the extreme values of the notch root residual stresses are limited by the yield point of material adjacent to the notch, that is, by the yield point of the base metal S_y (BM). In this analysis, the notch root residual stresses (σ_r) are presumed to be zero (after stress relief), + S_y(BM) (for the as-welded state) or - S_y(BM) (induced through a post-weld treatment).

The variation of ΔP with S_u HAZ is plotted in Fig. 18 for several assumptions of residual stress. Point T (ΔP = 1.57 kN) in Fig. 18 is the predicted range of load for SAE 1006 which compares well with an (extrapolated) average experimental value of 1.60 kN. Similarly for the HSLA spot welds Eq. 15 predicts ΔP = 1.4 kN which compares well with (extrapolated) an average experimental value of ΔP = 1.33 kN. The agreement between the model and experiment is rather good, and the assumptions regarding residual

stresses seem justified.

For a constant value of tensile (+) residual stress, increasing S_u (HAZ) results in larger values of ΔP; however, for the as-welded state, increasing S_u(HAZ) also implies increases in S_y(BM). Thus, the net result of higher base metal strength is to reduce the fatigue resistance through the development of higher tensile notch root residual stresses (T → T', in Fig. 18).

If S_u(HAZ) is not altered by stress relief or if the residual stresses can be reduced to zero without affecting S_u(HAZ), then stress relief would cause large improvements in fatigue resistance for both SAE 1006 and HSLA spot welds (T → 0, T' → 0' in Fig. 18). This improvement would be greatest for the higher strength HSLA material.

Inducing compressive residual stresses should cause a near doubling of the fatigue strength (T → C, T'→ C' in Fig. 18). Thus, alteration of residual stresses through a post weld treatment may substantially improve fatigue resistance. As attractive as residual stress control is, such improvements may not be permanent under variable load history service conditions.

Finally, if one considers the HAZ hardness to be controlled by the welding process, Fig. 18 suggests that for as-welded welds (which presumably have $\sigma_r \cong +S_y(BM)$, using a material with the least base metal yield strength (S_y(BM)) and a welding process which gives the highest hardness HAZ would give the greatest fatigue resistance at 10^7 cycles. Conversely, if compressive residual stresses could be induced, the optimal strategy would appear to be to use the highest yield point base metal (S_y(BM)) and least HAZ hardness.

6.4 The Predicted Effects of Load History

The predictions presented in this study have assumed constant amplitude loading. Actual service loads are more likely to be highly variable and

resemble the SAE bracket history. It is possible that the effects presented here which relate to material properties may prove incorrect for variable load histories. The improvements made through control of geometry would be expected to be independent of load history. Less severe notches should always result in an increased performance. However, residual stresses and applied mean stress effects may be very load history and life range dependent.

Figure 19 shows the influence of applied mean stress (R ratio) on the constant amplitude predictions using Eq. 15. Stress ratio has a very large influence on ΔP.

7. REFERENCES

1. Davidson, J. A., "A Review of the Fatigue Properties of Spot-Welded Sheet Steels," paper 830033 presented at the 1983 SAE International Congress and Exposition, Detroit, Michigan, February 1983.

2. Davidson, J. A. and Imhof, E. J., Jr., "A Fracture-Mechanics and System-Stiffness Approach to Fatigue Performance of Spot-Welded Sheet Steels," paper 830034 presented at the 1983 SAE International Congress and Exposition, Detroit, Michigan, February 1983.

3. Lawrence, F. V., Jr., Ho, N.-J., and Mazumdar, P. K., "Predicting the Fatigue Resistance of Welds," Ann. Rev. Mater. Sci., 1981, 11:401-25, pp. 401-425.

4. Creager, Matthew, "The Elastic Stress Field Near the Tip of a Blunt Crack," M. S. Thesis, Lehigh University, 1966.

5. Pook, L. P., "Approximate Stress Intensity Factors for Spot and Similar Welds," National Engineering Laboratory Report No. 588, April 1975.

6. Pook, L. P., "Approximate Stress Intensity Factors Obtained From Simple Plate Bending Theory," Engineering Fracture Mechanics, 1979, 12(4), 505-522.

7. Dugdale, D. S., Elements of Elasticity, Pergamon Press Ltd., Heddington Hill Hall, Oxford, 1967.

8. ACKNOWLEDGEMENTS

This study was supported in part by the University of Illinois Fracture Control Program. The specimens used and experimental results reported were donated by the General Motors Corporation through the kind efforts of Mrs. K. Ewing and Dr. A. Houchens of the General Motors Technical Center.

TABLE 1

WELDING PROCEDURES

Material and Weld Schedule		Electrode Force (kN)	Hold Time (Cycles)	Weld Time (cycles)	Weld Current (kamps)
SAE 1006	4	2.66	30	12	8.7
SAE 960X	3	3.56	30	20	11.0
SAE 960X	4	3.56	30	20	12.7
SAE 960X	5	3.56	30	20	15.8

TABLE 2

COMPARISON OF EXPERIMENTAL AND PREDICTED LOAD RANGE
AT 2×10^6 CYCLES FOR TENSILE-SHEAR SPOT WELDS

Material	S_y(MPa)	S_a(MPa)	S_uHAZ[b] (MPa)	W(mm)	t(mm)	D(mm)	Load Range at 2×10^6 Cycles (kN)	
							observed	predicted (Eq.7)
SAE 1006	186	317	655	38.1	1.27	5.84	2.22	1.80
SAE 1006 (GALV.)	248	324	655	38.1	1.27	5.84	2.22	1.70
SAE 950X (8118)[a]	381	458	896	50.8	2.06	6.35	2.13	2.06
SAE 950X (8125)[a]	381	458	896	50.8	2.06	8.10	2.80	2.69
SAE 950X (8131)[a]	381	458	896	50.8	2.06	9.65	2.89	3.21
SAE 950X (8135)[a]	381	458	896	50.8	2.06	11.05	3.11	3.67
SAE 950X (8118)[a]	381	458	896	25.4	2.06	6.15	1.91	1.94
SAE 950X (8131)[a]	381	458	896	25.4	2.06	9.65	1.87	2.97
SAE 960X	400	476	896	38.1	1.27	5.84	1.83	1.56
SAE 960X (GALV.)	400	476	896	38.1	1.27	5.84	2.00	1.56

a. Results reported by Davidson and Imhof (2).
b. Estimated from microhardness measurements in heat-affected-zone.

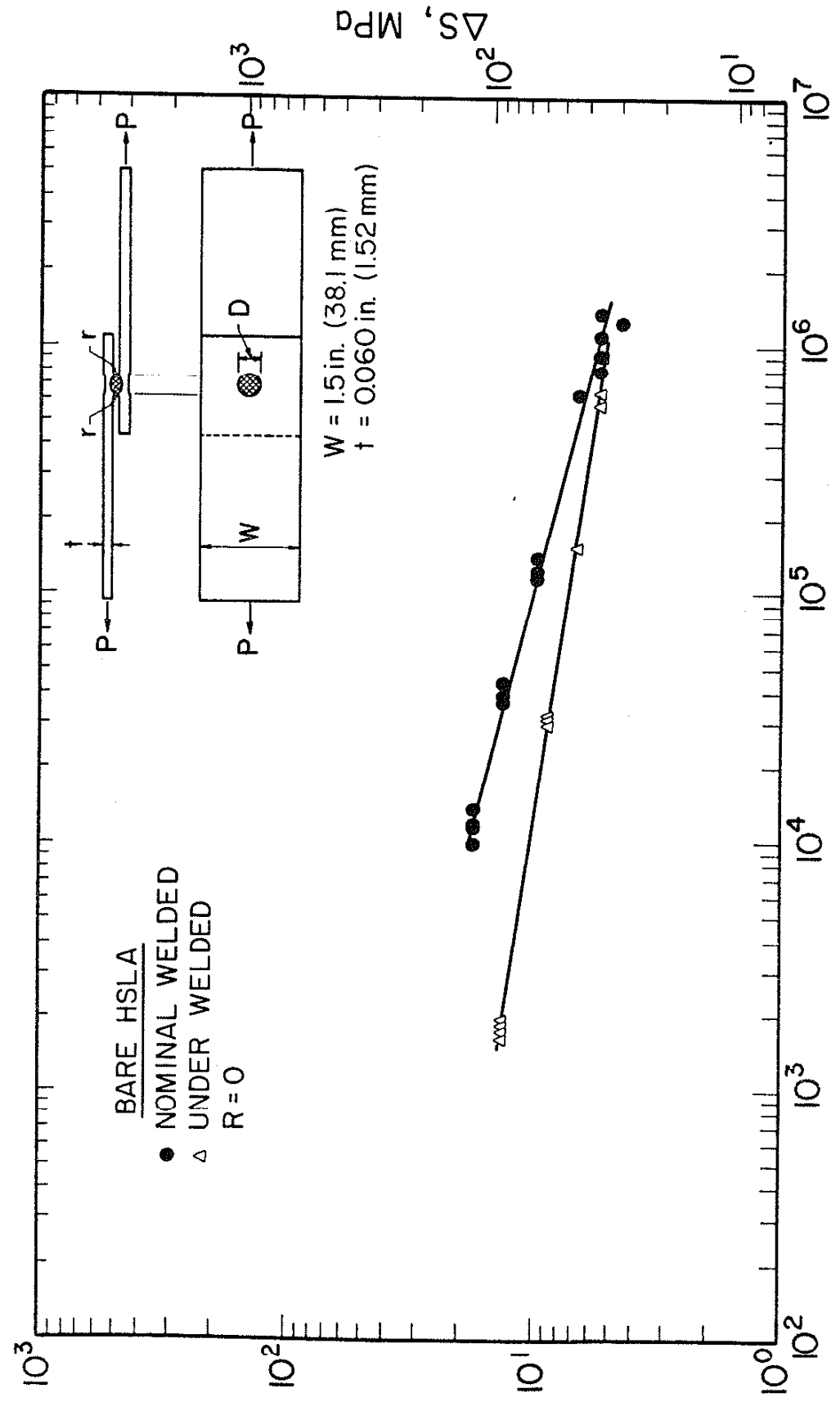

Fig. 1. S-N Diagram for Ungalvanized SAE 960x (Bare HSLA) Tensile-Shear Spot Weld. Solid Symbols Are for Welding Condition #4. Open Symbols Are for Welding Condition #3. Testpieces Welded with Welding Condition #3 Usually Exhibit Interfacial Failure and Hence, Lesser Fatigue Resistance. ΔS Is Equal to ΔP/wt.

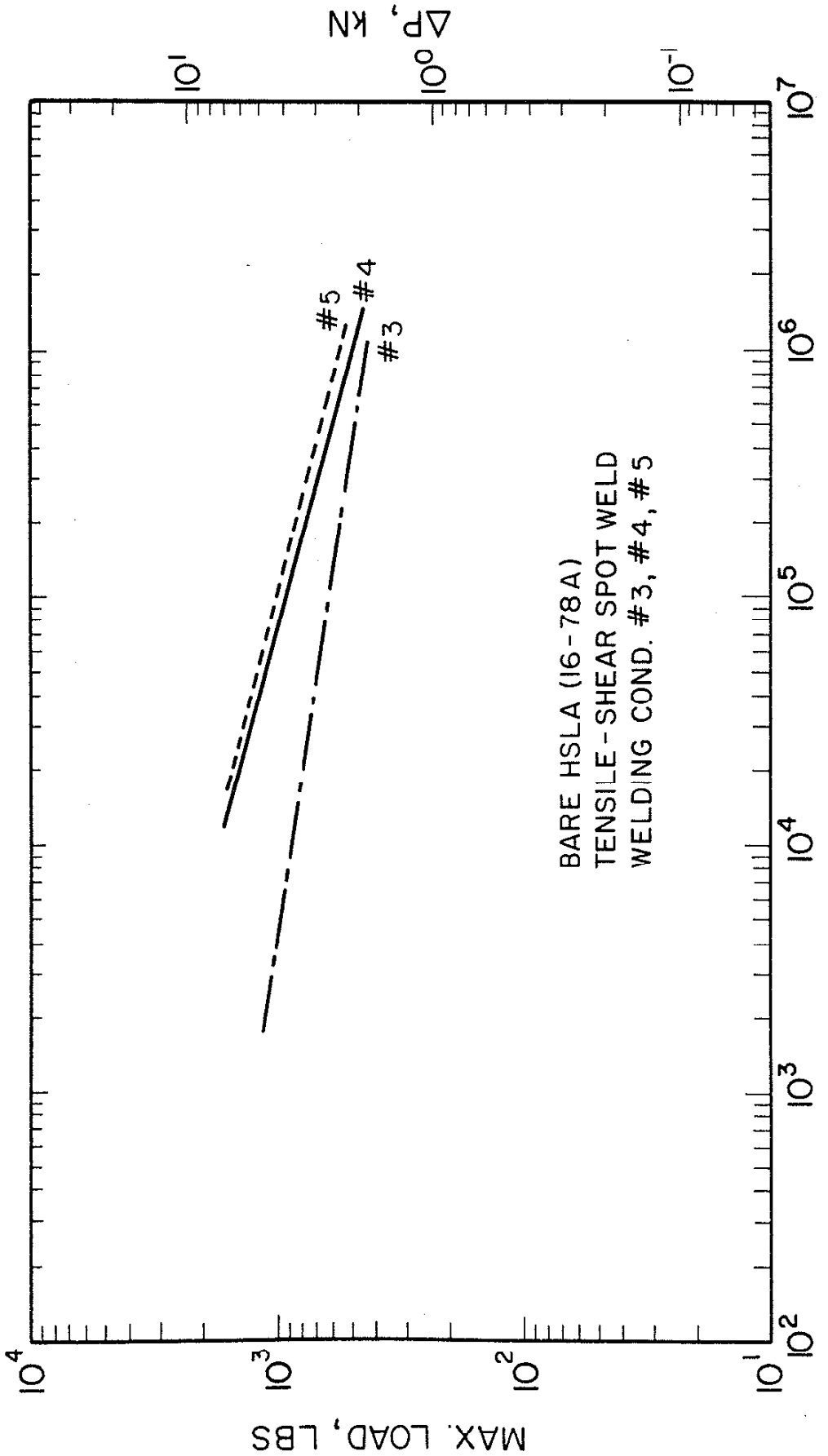

Fig. 2. Summary of the Best-Fit Lines to the Test Data for the Welding Conditions Studied for Ungalvanized SAE 960x Tensile-Shear Spot Weld Specimens.

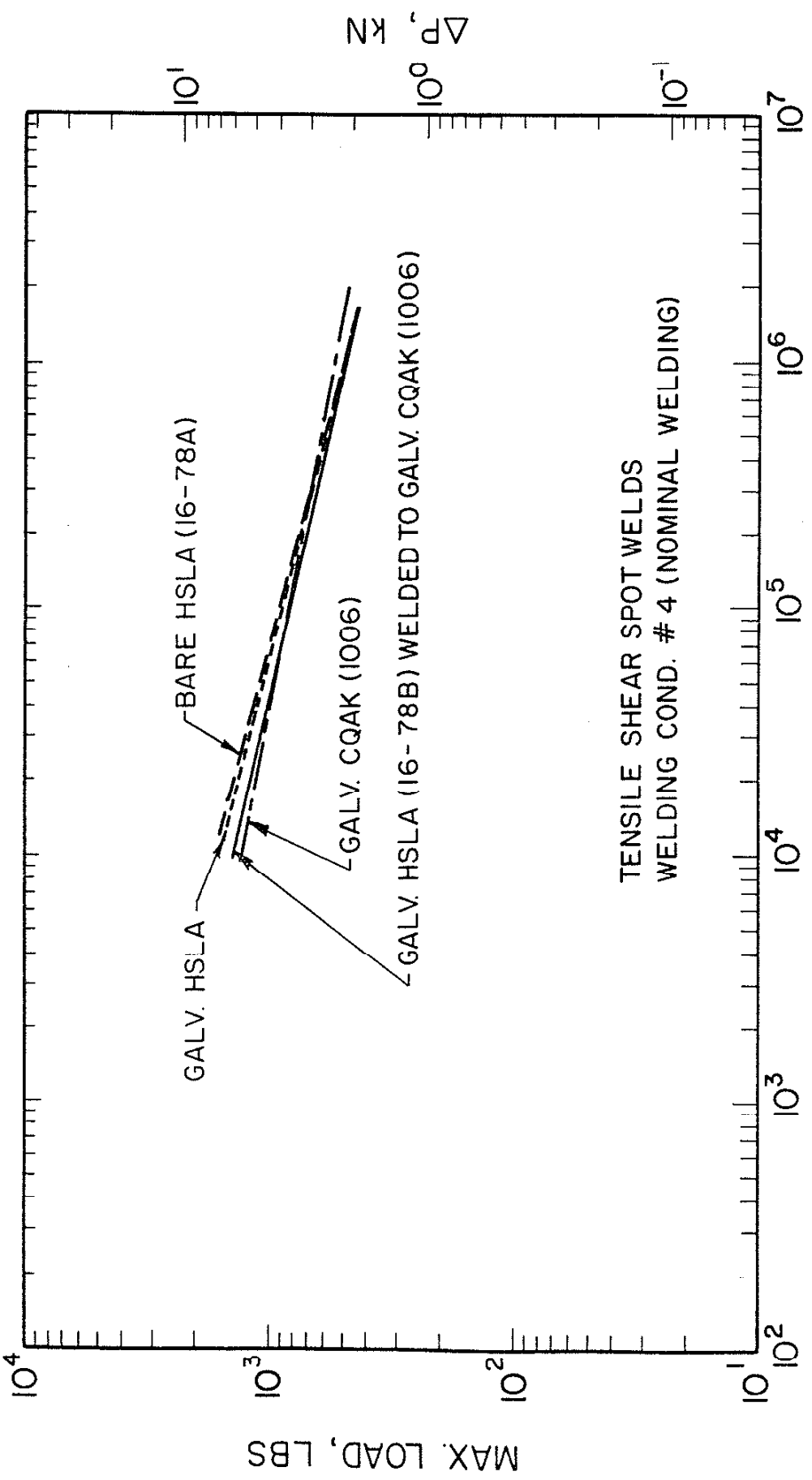

Fig. 3. Summary of the Best-Fit Lines to the Test Data for the Materials Studied Using Tensile-Shear Spot Weld Specimens, Welding Condition #4.

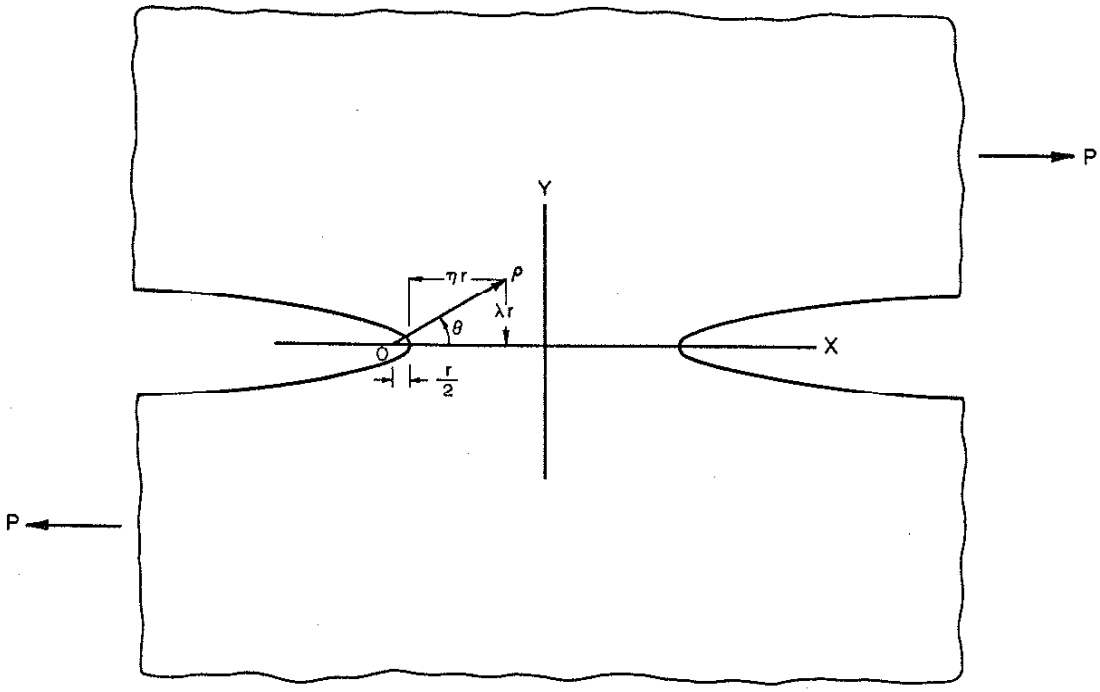

Fig. 5a The Hyperbolic Blunt Crack with Finite Crack Tip Radius (r).

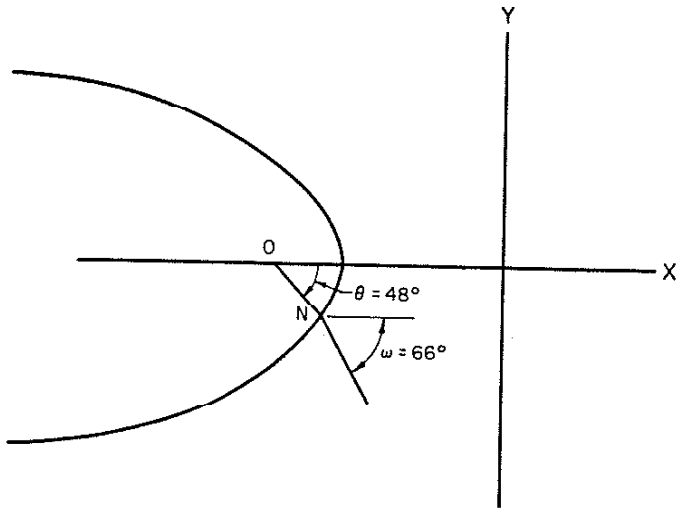

Fig. 5b The Initial Angle of Crack Growth.

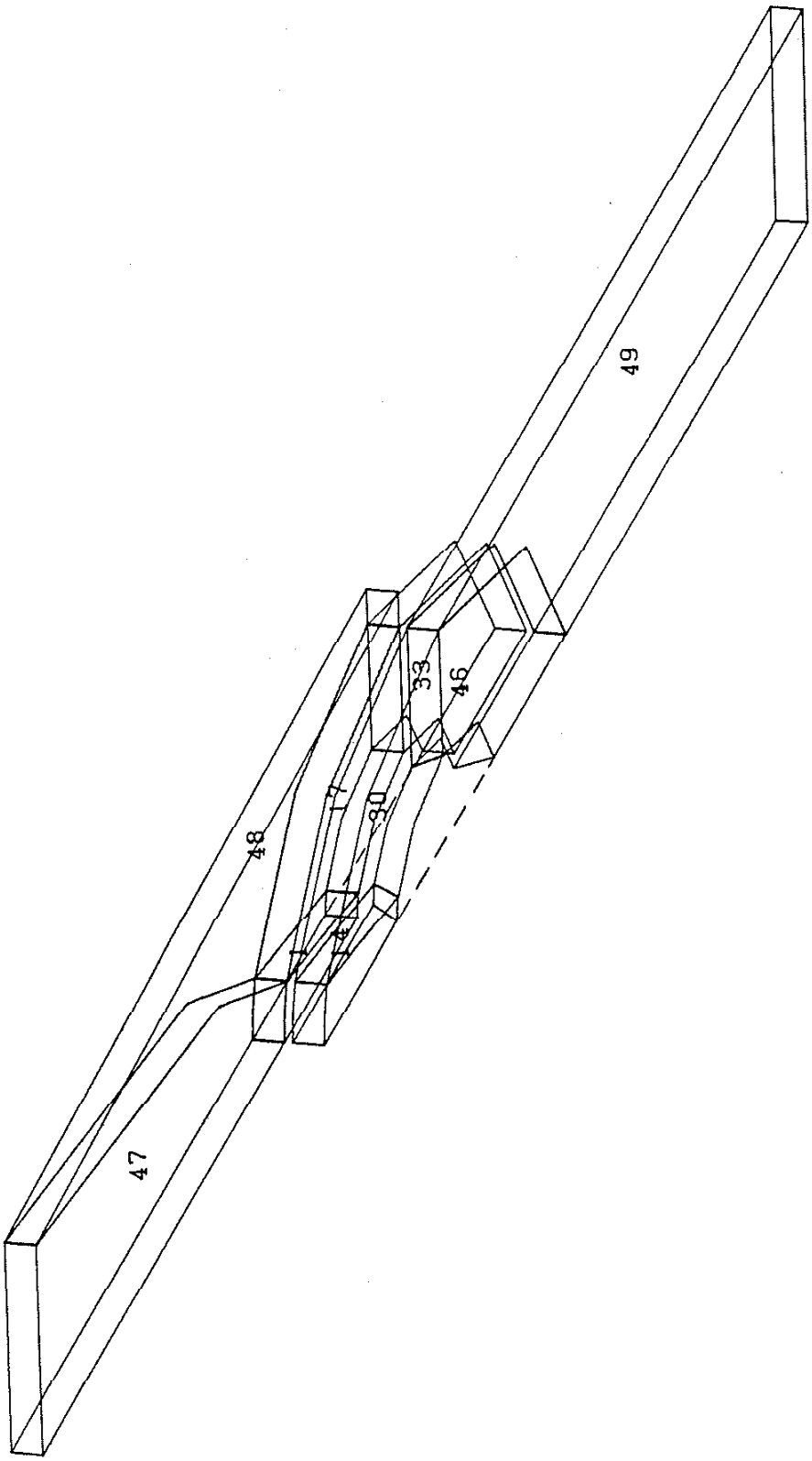

Fig. 6. 3-D Finite Element Coarse Mesh of Tensile-Shear Weld.

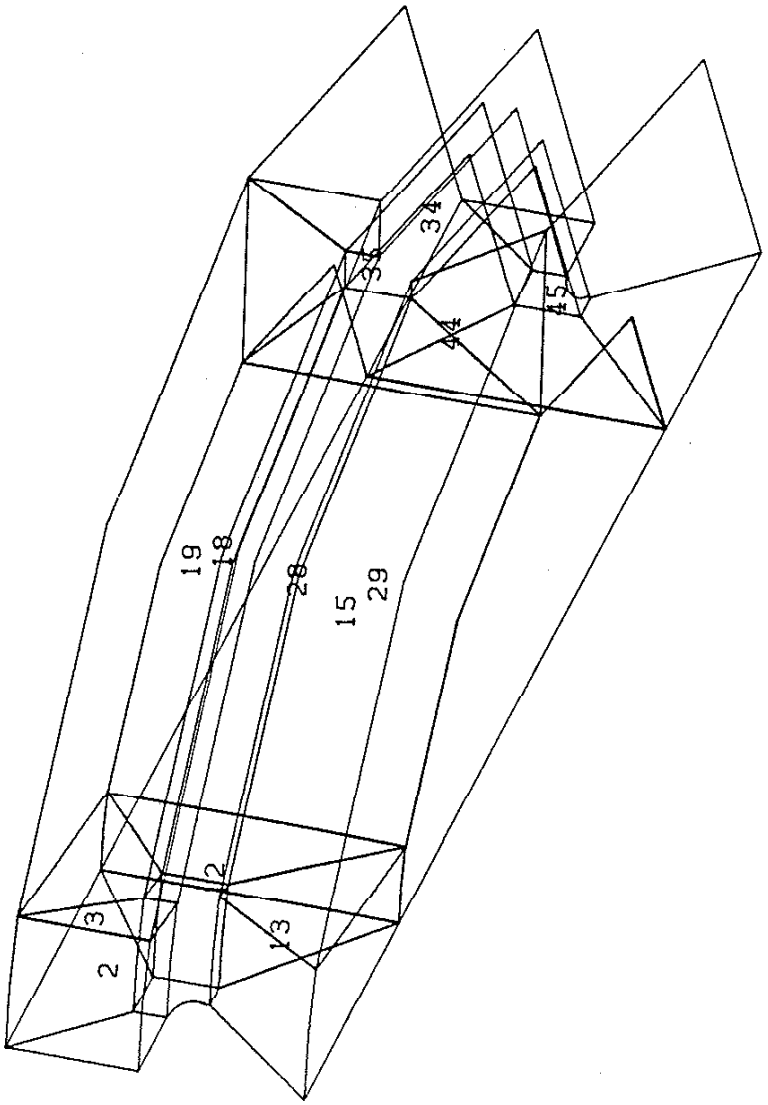

Fig. 7. Enlarged 3-D Finite Element Mesh of the Nugget.

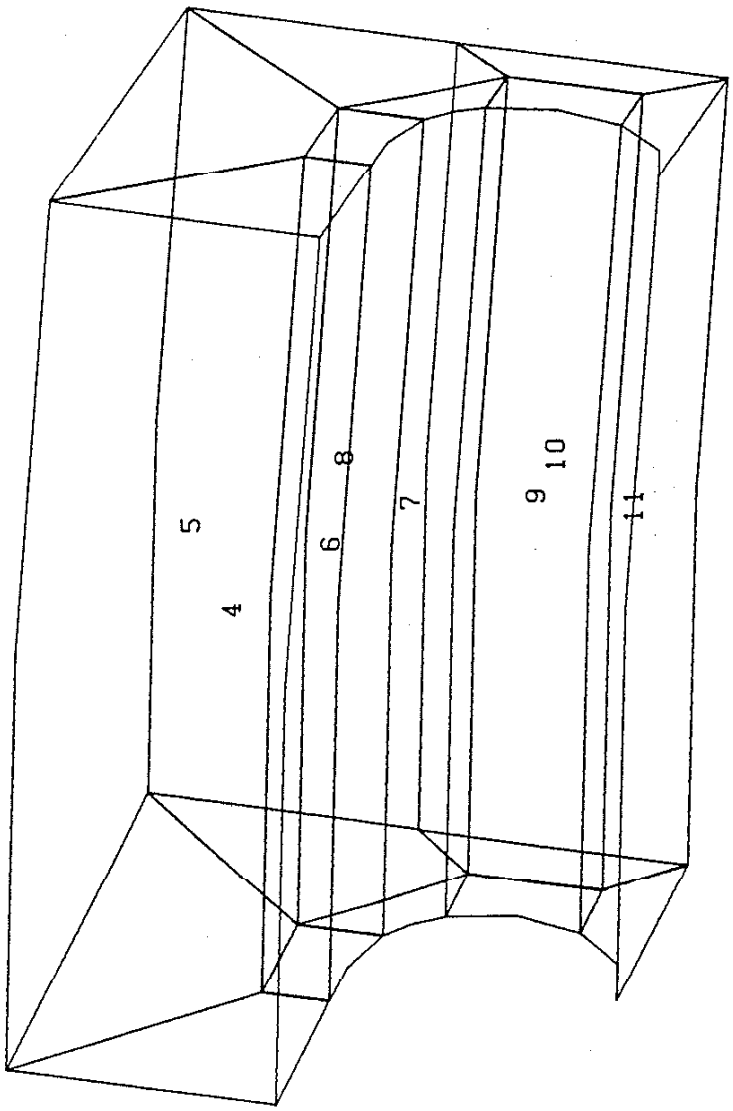

Fig. 8. Refined 3-D Finite Element Mesh at the Notch Root.

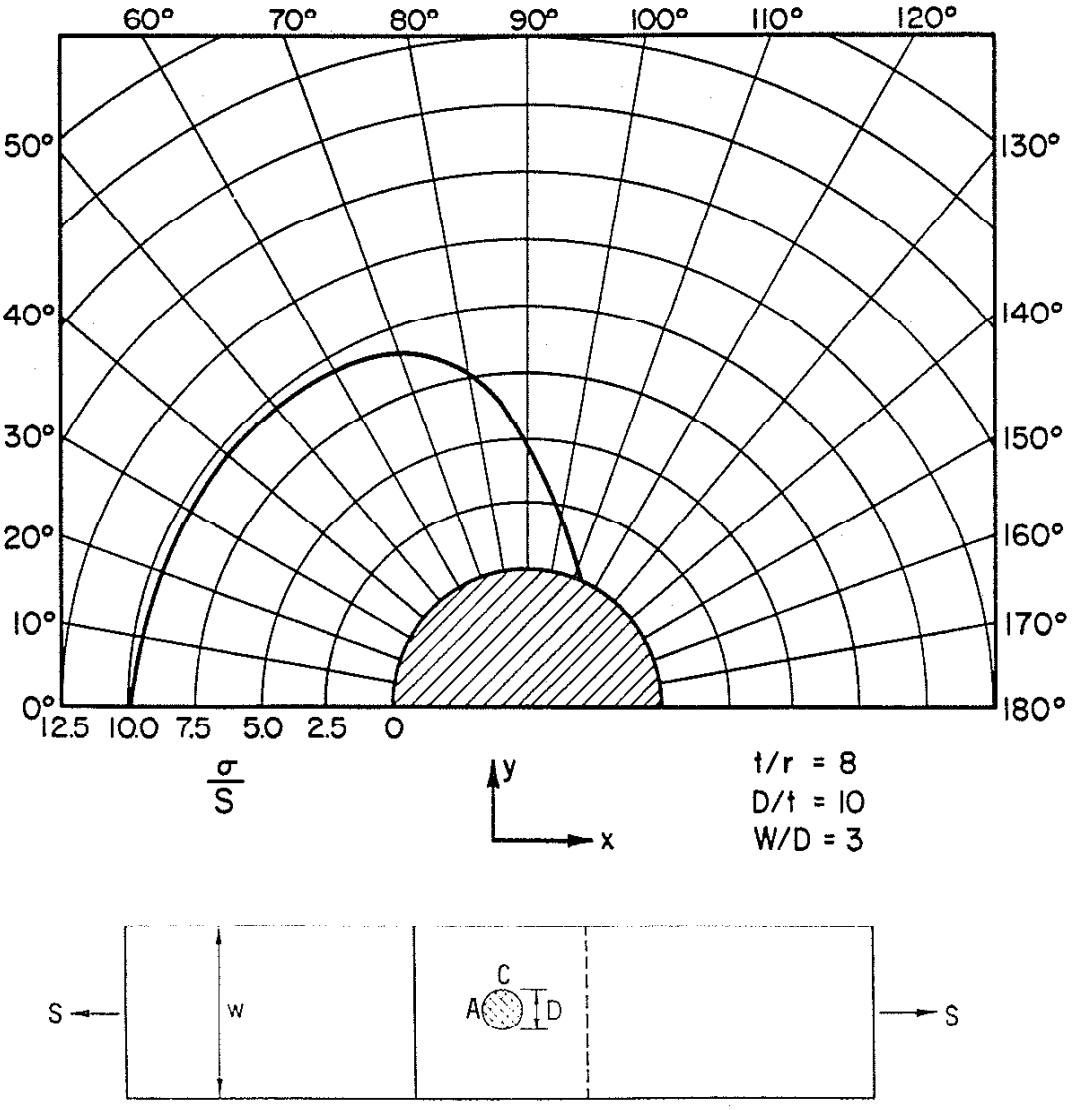

Fig. 9. Principal Stress Distribution Around the Nugget Circumference.

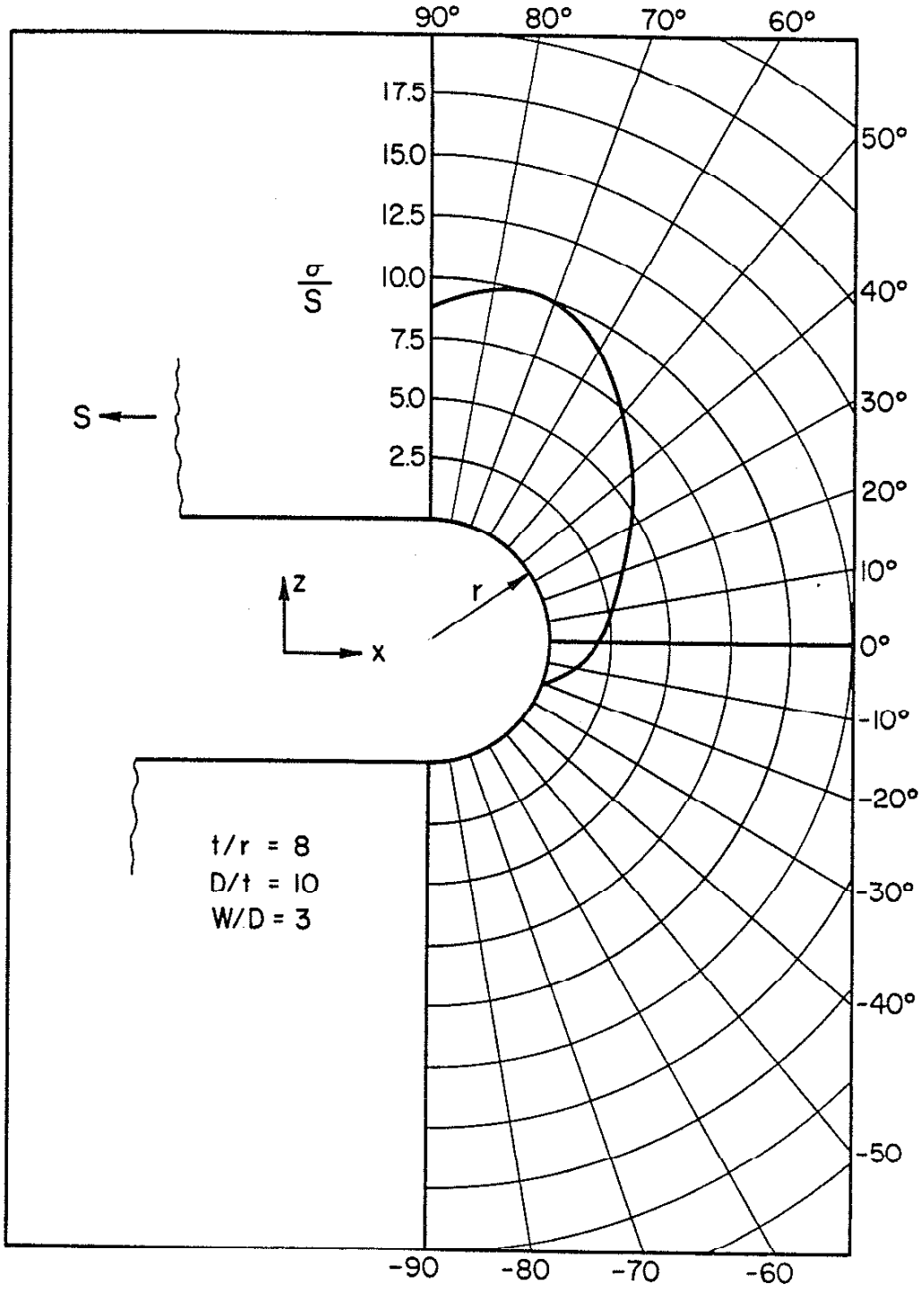

Fig. 10. Principal Stress Distribution at the Notch Root.

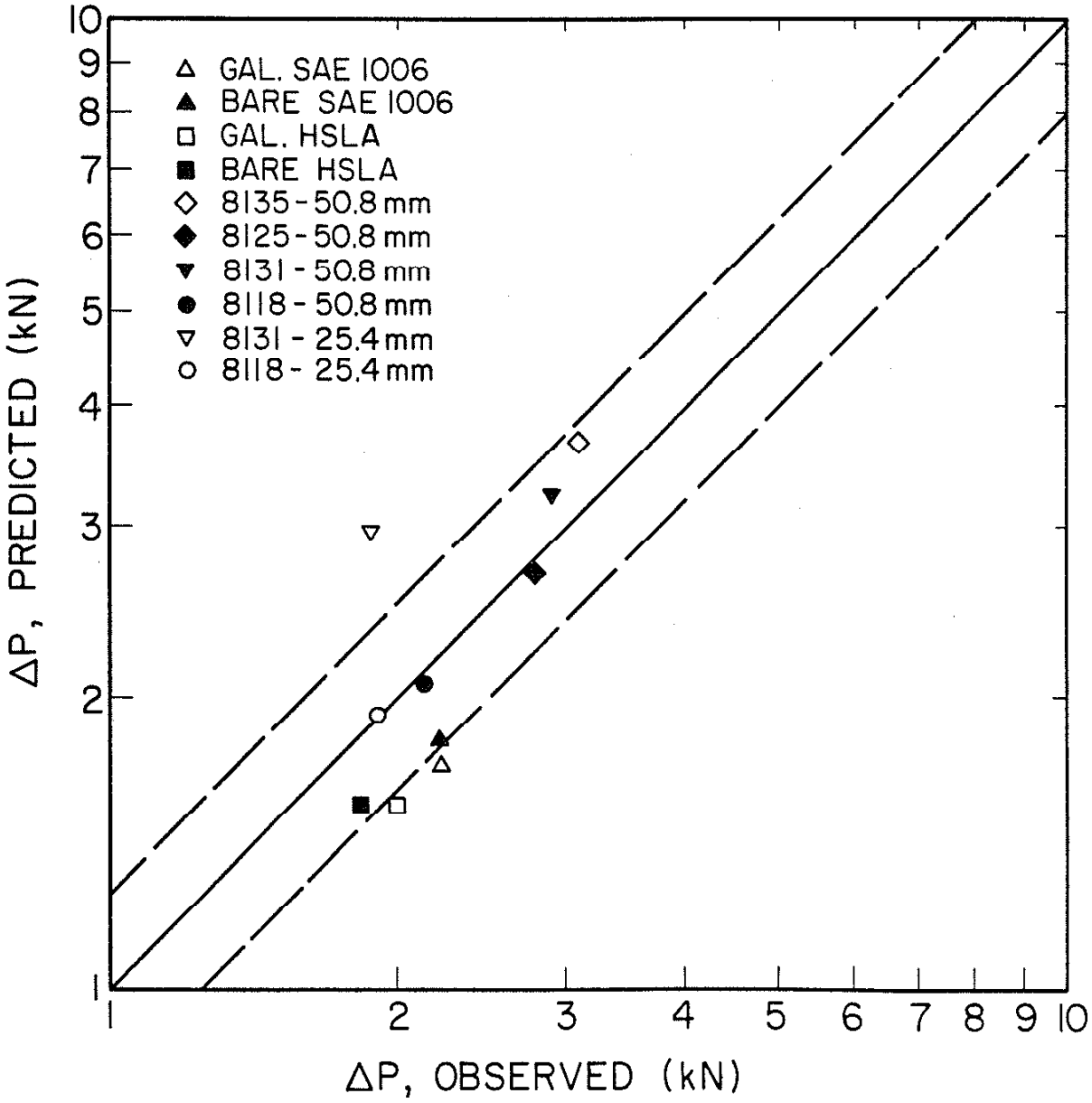

Fig. 12. Comparison of Predicted and Observed Total Load Range (ΔP) for Tensile-Shear Spot Weld at 2 x 10^6 Cycles under R = 0 Loading Conditions. Results from Present Study and Davison and Imhof (2).

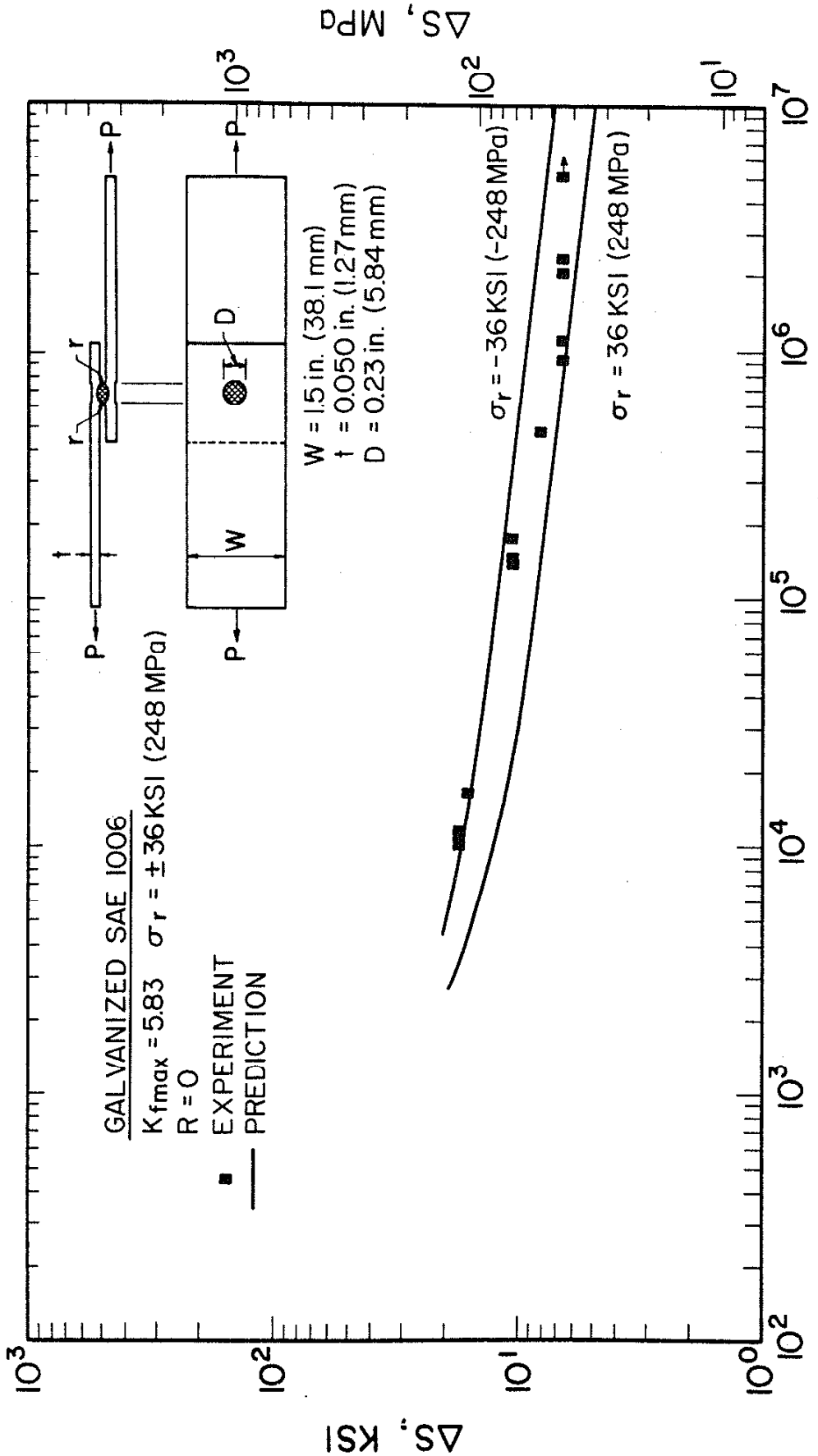

Fig. 13. Total Fatigue Life Predictions and Experimental Results for Galvanized SAE 1006 Tensile-Shear Spot Welds, Welding Condition #4.

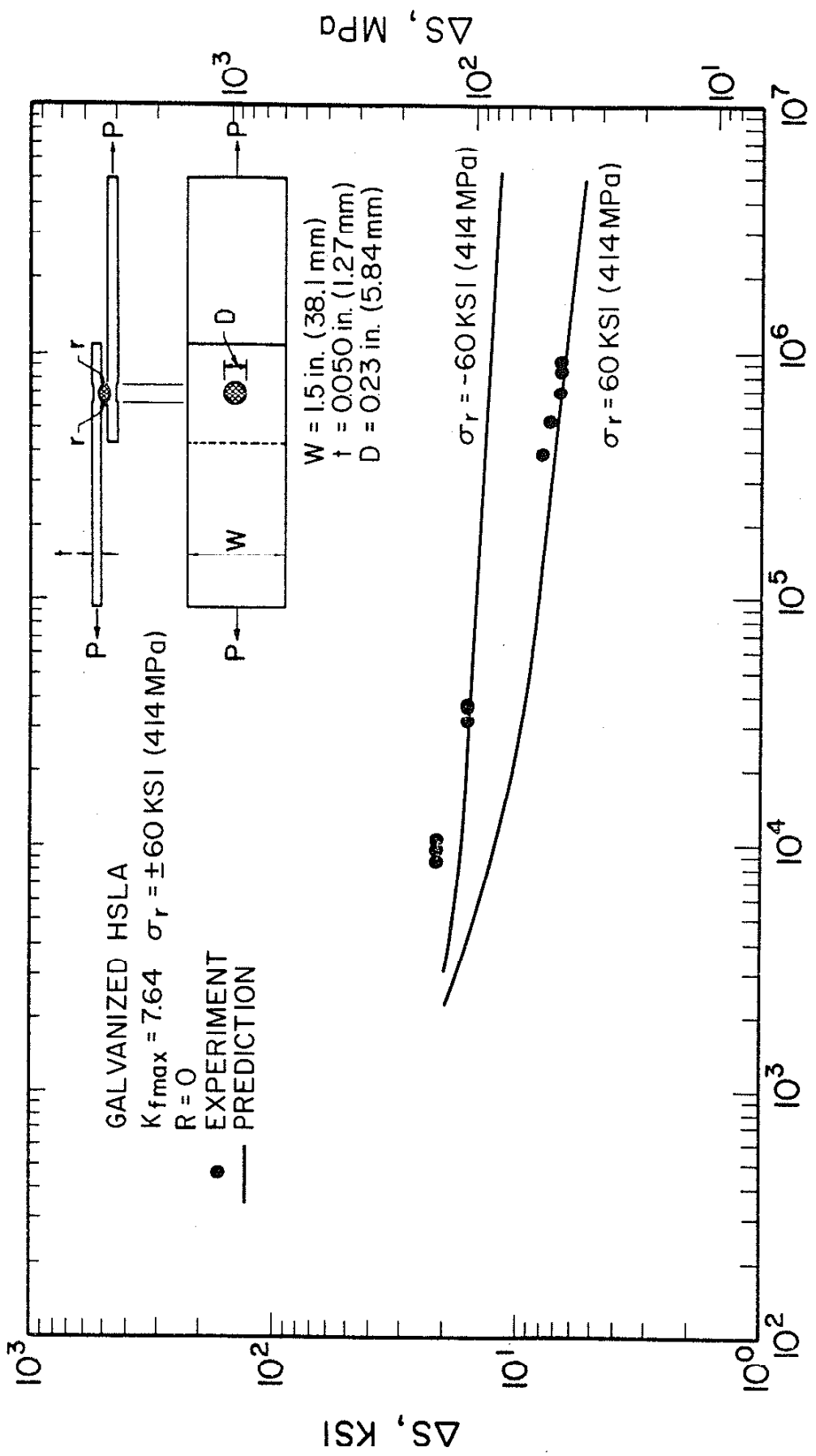

Fig. 14. Total Fatigue Life Predictions and Experimental Results for Galvanized SAE 960x (HSLA) Tensile-Shear Spot Welds, Welding Condition #4.

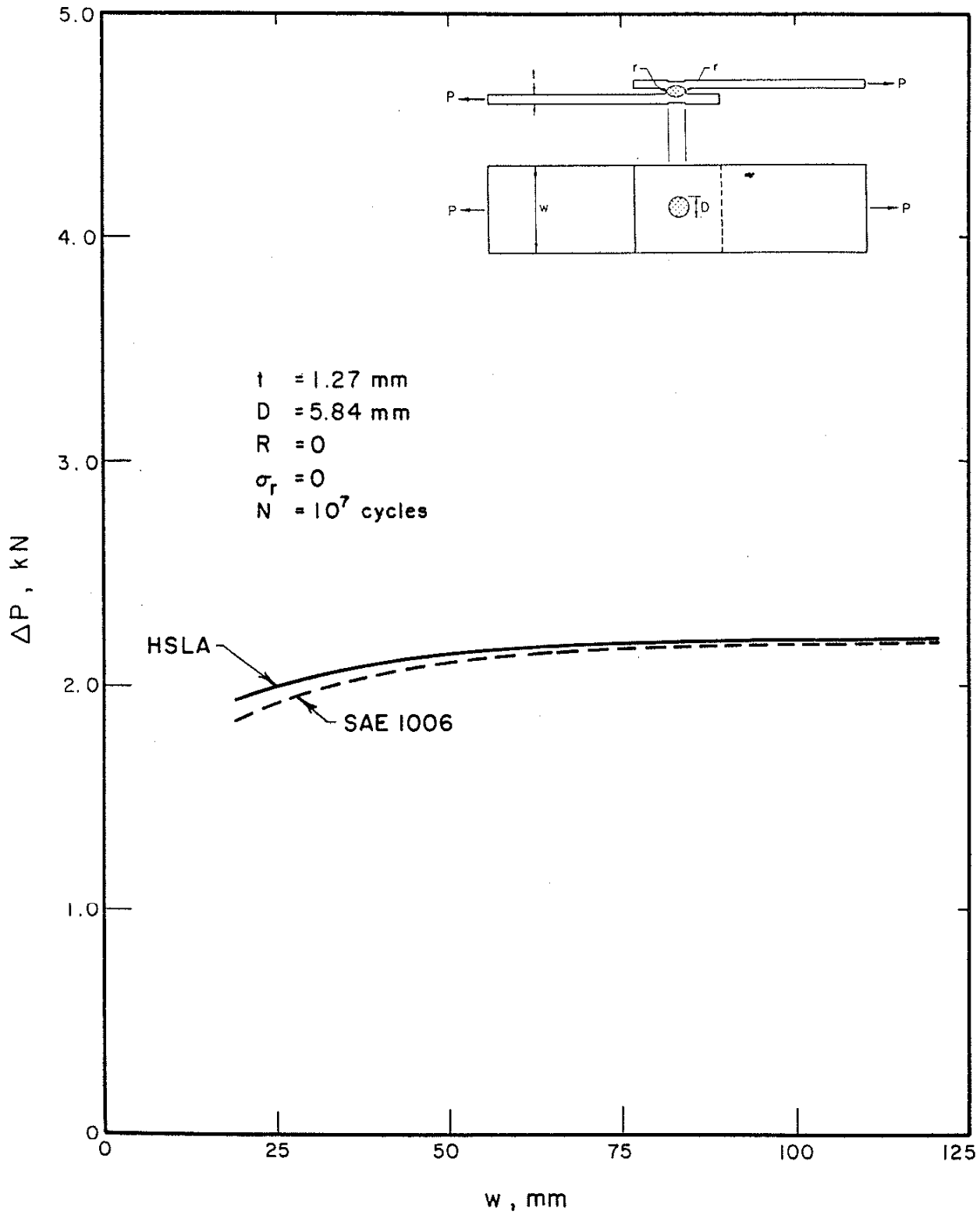

Fig. 15. Predicted Effect of Sheet Width (W) on the Load Range (ΔP) for SAE 960x and SAE 1006 Tensile-Shear Spot Welds.

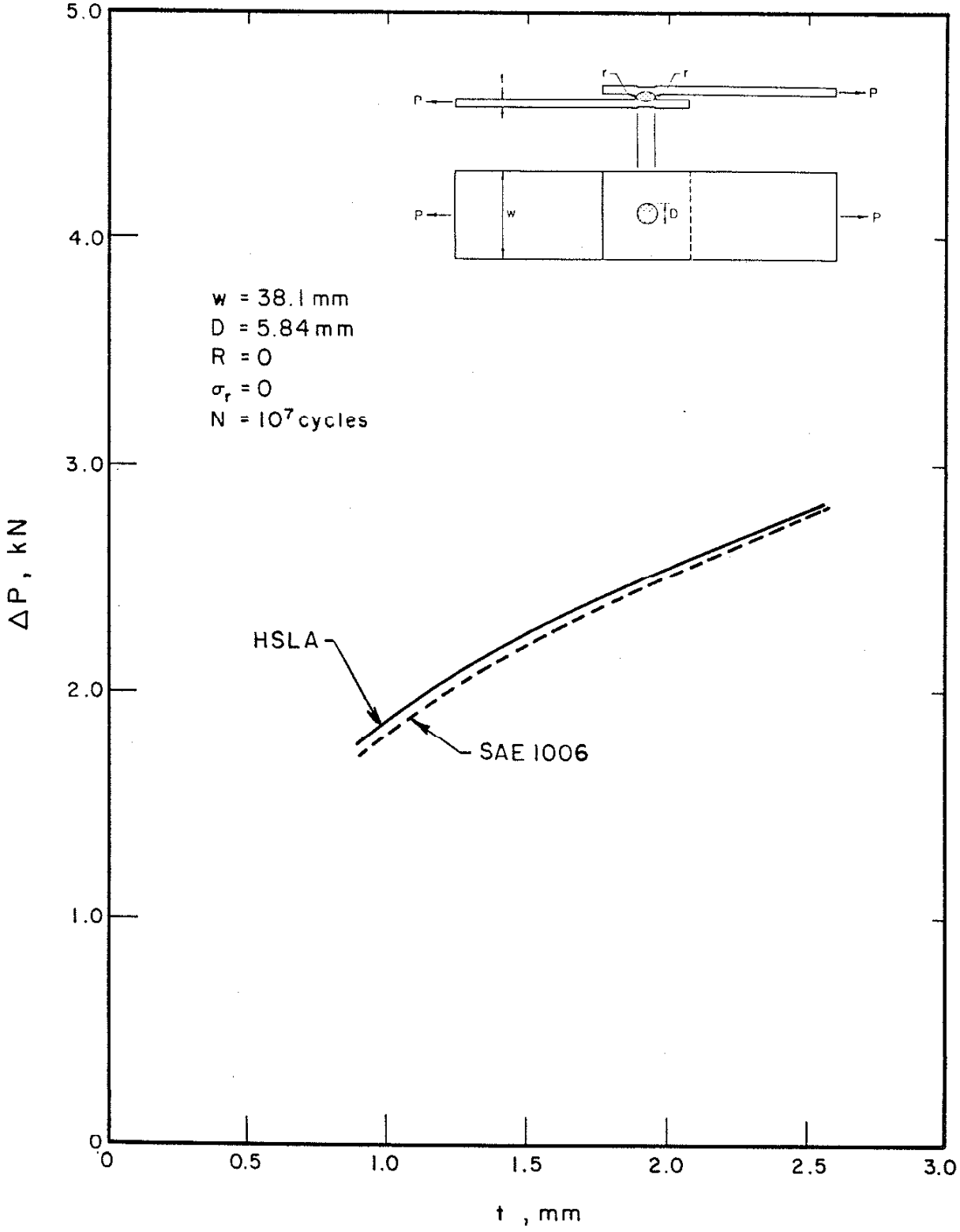

Fig. 16. Predicted Effect of Sheet Thickness (t) on the Load Range (ΔP) for SAE 960x and SAE 1006 Tensile-Shear Spot Welds.

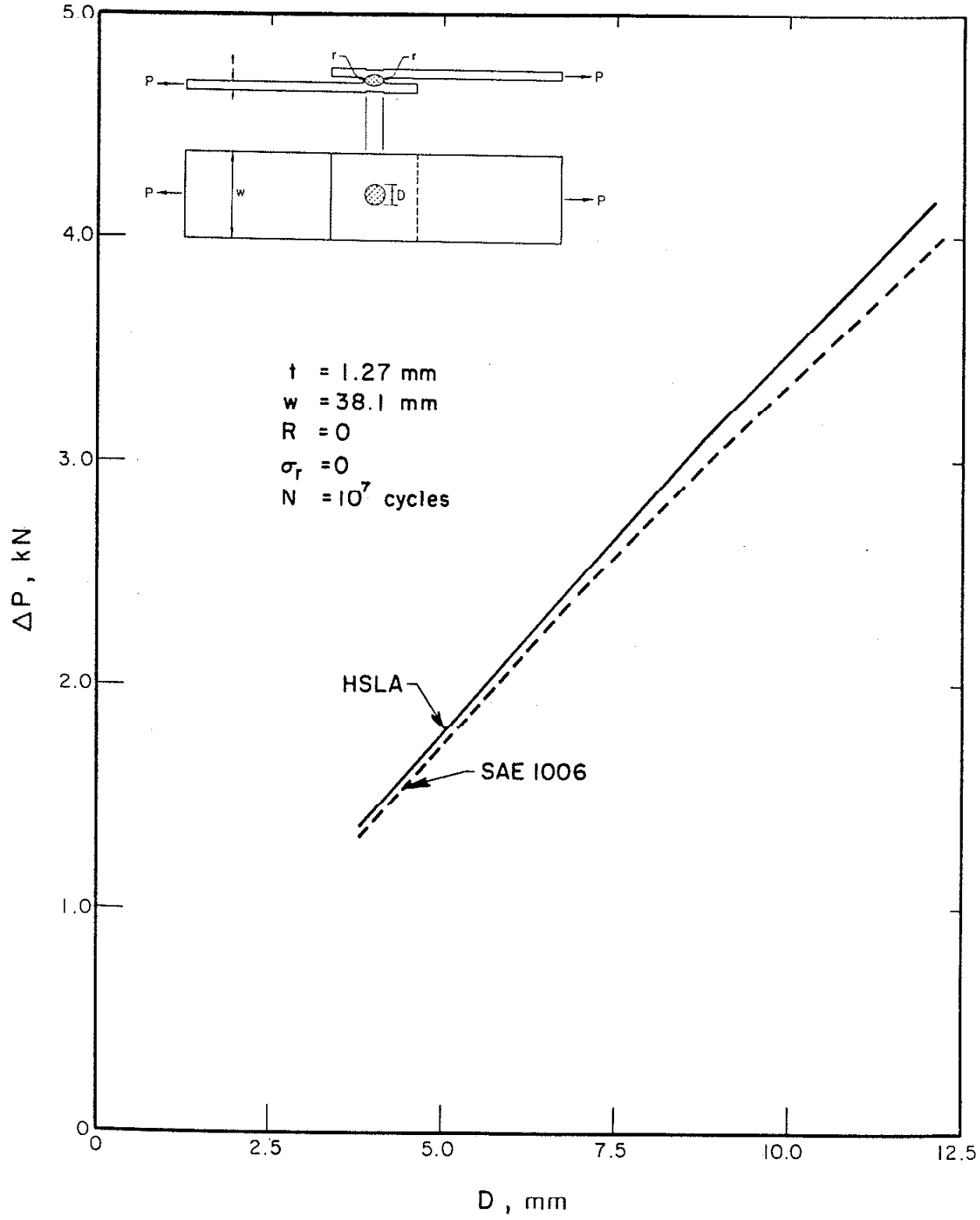

Fig. 17. Predicted Effect of Nugget Diameter (D) on the Load Range (ΔP) for SAE 960x and SAE 1006 Tensile-Shear Spot Welds.

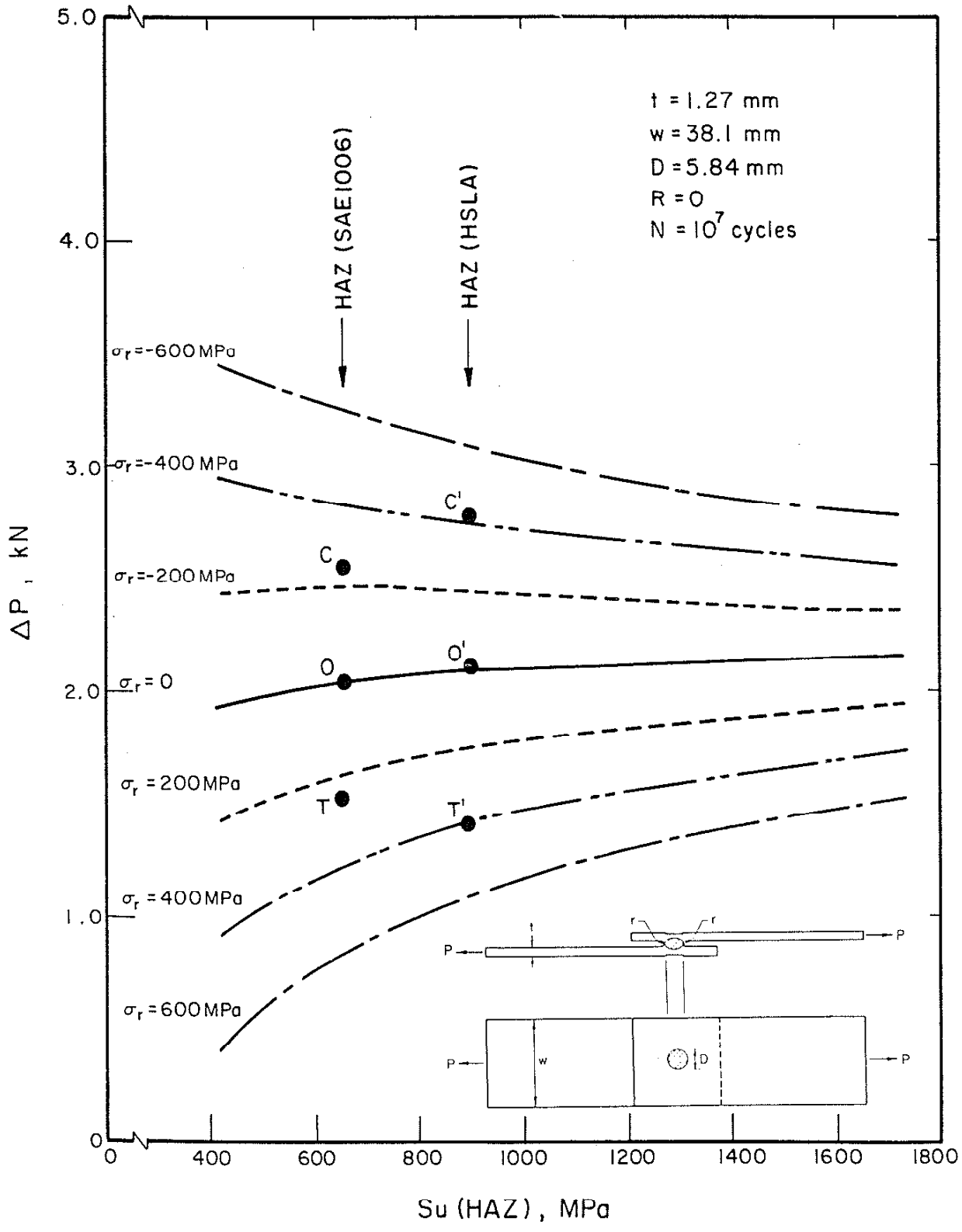

Fig. 18. Variation of Predicted Load Range (ΔP) at 10^7 Cycles with Heat-Affected-Zone Tensile Strength (Su) for the Tensile-Shear Spot Weld. Various Assumptions of Residual Stress Are Plotted.